Accepted Manuscript

Halloysite nanotube and its firing products: structural characterization of halloysite, metahalloysite, spinel type silicoaluminate and mullite

L. Andrini[1], R. Moreira Toja[2,3], M.S. Conconi[2,3], F.G. Requejo[1,4], **N.M. Rendtorff[2,3]***

[1].   Instituto de Fisicoquímica Teórica y Aplicada (INIFTA): (UNLP-CONICET La Plata), 64 y Diagonal 113 (1900), La Plata, Argentina.

[2].   Centro de Tecnología de Recursos Minerales y Cerámica (CETMIC): (CIC-CONICET-CCT La Plata), Camino Centenario y 506, C.C.49 (B1897ZCA), M.B. Gonnet, Argentina.

[3].   Dpto. de Química, Facultad de Ciencias Exactas, Universidad Nacional de La Plata, UNLP, 47 y 115 (1900), La Plata, Argentina.

[4].   Dpto. de Física, Facultad de Ciencias Exactas, Universidad Nacional de La Plata, UNLP, 49 y 115 (1900), La Plata, Argentina.

*Corresponding author: rendtorff@cetmic.unlp.edu.ar

Highlights

- Halloysite nanotubes have many applications; a thermal pre-treatment is employed in many of them.
- Thermal, structural and microstructural description was carried out up to 1400°C.
- Al- Near edge absorption spectroscopy (XANES) was employed for local structure.
- Loss of crystalinity, tube morphology retention were observed.
- A multiple Al-Coordination for Metahalloysite was determined.

Abstract

Halloysite and its heating products demand attention due to its multiple technological applications, and in particular for its natural nanostructure. The purpose of this paper is to present a structural characterization of these materials and its firing products up to mullite. To achieve this objective, the techniques of conventional X-ray diffraction (XRD) and X-ray absorption near-edge structure (XANES) were used, in addition to scanning electron microscopy (SEM), and simultaneous thermogravimetric and differential thermal analysis (DTA-TG). SEM has allowed to prove that the nanotubular morphology (acicular) of halloysite was retained for all temperatures (500, 800, 1100 and 1250 °C). For the temperatures between 500 and 800 °C the metahalloysite phase was identified. The 1100 °C fired samples presented the spinel aluminosilicate phase. Finally, after high temperature treatments the mullite phase was detected as the only aluminum containing crystalline phase accompanied by cristobalite and glassy phase. The XANES spectra

confirmed the octahedral aluminum coordination in native halloysite, this coordination was progressively lost with the thermal treatments giving place to the presence of the four folded coordination. In the intermediate treatments, the so called metahalloysite phase, presented some three and five coordination slight contributions. Particularly, the metahalloysite Al K XANES spectra were not reported before.

Key Words: halloysite; thermal behavior; structure; XANES

1. Introduction

The halloysite has the same theoretical chemical composition as kaolinite except for its higher water content. The ideal unit formula for halloysite-(7 Å) and halloysite-(10 Å) is $Al_2Si_2O_5(OH)_4.nH_2O$ where n = 0 and 2, respectively [1,2]. However, the chemical composition is subject to little variation. The common presence of impurities in halloysitic samples makes it difficult to assess the chemical composition of the halloysite [3–6].

The particle morphology of halloysite appears to be related to crystallization conditions and geological occurrences [4,7–13].

Several halloysite morphologies have been described: tubular (long or short); pseudo spherical and spheroidal; platy or tabular; fiber like, prismatic; cylindrical, including mathematical models to explain the conformation geometry of this mineral [14]; disk shape; spherulitic, crumpled lamellar halloysite morphologies has been defined as well. Finally, lath, scroll, and glomerular morphologies have been also described. But because tubular halloysite present a marked technological and economic interest is that its attract special attention in the basic research field [15–21].

Based on transmission electron microscopy (TEM) observations, a model for halloysite tube development from plated kaolinite was proposed [22,23]. The process appears to have been initiated by a progressive alteration of kaolinite inducing a loss of structural rigidity at points along the crystal, interpreted as hydration to halloysite. As alteration of kaolinite progressed, the halloysite developed, on and attached to, a kaolinite plate curled smoothly, rolling up part of the plate [22].

Unlike the clay minerals that have a platy morphology, halloysite $Al_2(OH)_4Si_2O_5.2H_2O$, which is a hydrated polymorph of kaolinite, has a unique tubular morphology with a mesoscopic (2–50 nm) or even macroscopic (>50 nm) lumen (the inner cavity of the tubular halloysite particle). The tubular morphology of halloysite results from the wrapping of halloysite layers that is driven by a mismatch between the oxygen-sharing tetrahedral SiO_4 sheet and the adjacent octahedral AlO_6 sheet in the 1:1 layer under favorable crystallization conditions and geological occurrences. Generally, tubular halloysite is approximately 0.02–30 μm long and has an external diameter of 30–190 nm and an internal diameter (lumen) of 10–100 nm. These sizes vary in different halloysite deposits [6,7,24–26]. The nano-sized tubular structure and the mesoporosity (or even macroporosity) of halloysite make it suitable for use as a nanoscale reactor for biomineralization, an adsorbent for pollutants, an additive for polymer nanocomposites, and a carrier for the controlled release of protective agents. In particular, the lumen size of halloysite is greater than 10

2

nm, which is sufficiently large to accommodate various guests [27,16,28,17,29,24,21,30]. Or even employed as a nano-reactor [15].

As has been reported [31], halloysite contains two types of hydroxyl groups, inner and outer hydroxyl groups, which are situated between layers and on the surface of the nanotubes, respectively. Due to the multi-layer structure, most of the hydroxyl groups are inner groups and only a few hydroxyl groups are located on the surface of halloysite nanotubes. This surface is mainly composed of O–Si–O groups, and the siloxane surface can be confirmed from Fourier Transform Infrared spectra (FTIR), in which the very strong absorption of O–Si–O (ca 1030 cm^{-1}) is observed. Consequently, compared with other silicates such as kaolinite and montmorillonites, the density of surface hydroxyl groups of halloysite nanotubular is much smaller [31].

As similar clay minerals, halloysites may be characterized by a number of techniques, including X-ray diffraction (XRD), thermal analyses (TG and DTA), and infrared (IR) or Raman spectroscopy. The transmission and scanning electron microscopies (TEM and SEM) are also used to observe the crystalline morphological arrangement [17,19,22,32,33].

As mentioned before, and besides the morphological aspects, from the mineralogical point of view halloysite is similar to kaolinite. It might present one more water layer that is lost at low temperatures (this is known as the 10 Å – 7 Å dehydration). The thermochemical processes are similar between kaolinite and halloysite.

The classic papers of Brindley and Nakahira reported for the first time a systematic study of phase transformations for the kaolinite–mullite series [34,35], and measured the transformation temperature for a model material. The actual temperature transformations can be evaluated by several thermal analysis techniques, such as thermogravimetry, differential thermal analysis, calorimetry, etc. [36]. The particular properties, like chemical composition, particle size, transformation temperature, etc., of each raw natural material depend on its different geochemical constitutions including impurities [36].

The kaolinite–mullite series was recently studied by means of powder neutron diffraction [37] and the metakaolinite (MK) formation was studied by NMR [38–40]. The mechanisms were proposed and corroborated by the use of combined structural and thermal techniques.

The kaolinite (K) dehydroxylation occurs through a three dimensional diffusion process, with the formation of an amorphous product identified as metakaolinite ($Al_2Si_2O_5$), this process is completed above ~650 °C. An analogy can be carried out for the halloysite (H) dehydroxylation.

The metahalloysite (MH) retains its short-range order to at least ~980 °C. The formation of nanometer size and randomly oriented needle-like mullite (≈980–992 °C), primary mullite (Mi), side by side with a cubic phase, Si–Al spinel (SAS), and amorphous silica-rich at around ≈983 °C (G) can be identified [39,41,42]. The Mi formation is incipient. From ≈ 1136 °C growth of mullite (Mi) crystals occurs and at T ≥ 1200 °C crystallization of high temperature cristobalite (SiO_2) from a Si-rich amorphous phase takes place. Between 983 °C and 1136 °C, it is correct to assume that the amount of SAS will be higher than Mi. Additionally, in the Si-rich amorphous phase formed at kaolinite–mullite interfaces secondary mullite (Mii) crystallization occurs (~1300 °C). The impurities in the starting kaolin can induce a liquid phase during firing [37]. Since the mid-nineties *in situ* experiments using synchrotron radiation diffraction on kaolin specimens were made

3

[43,44]. They studied the kinetics of mullite formation in the 1300–1400 °C temperature range and the kinetics of dehydroxylation of two kaolin specimens in the 500–700 °C temperature range.

The stoichiometry of the metahalloysite (MH) corresponds with the halloysite (H) one, secondly the SAS stoichiometry remains undefined, and finally mullite varies in a small range [45]. The vitreous phase (G) belongs to the alumina-silica system, with high silica concentration, accompanied by the different impurities, principally alkali (K and Na), earthen alkali (Ca and Mg), iron oxide, or titania.

Several transformations occur in halloysite, which will be characterized in the present study. These transformations can be represented by the following scheme:

H→MH (400-700 °C)   (1)
MH→SAS (+G) (≈980 °C)   (2)
MH→Mi (+G)   (≈980 °C)   (3)
SAS→Mii+G (1130-1300 °C)   (4)
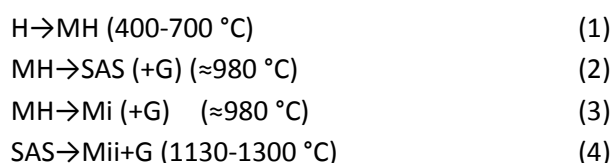
The local crystalline nature of MH and SAS is different, and it is one of the points that will be demonstrated in this work. MH presents a short range ordering, but no long range order and therefore no XRD Bragg reflections are present. On the other hand, SAS presents some short range order but the crystalline domains (crystallites) are nanosized and therefore it is difficult to evaluate this phase using XRD analysis [41,42,46–48]. Generally, it is identified by the presence of three wide bands at 2θ = 37, 46 and 67 ° [41]. In recent years, White *et al*. used the X-ray Absorption Near Edge Structure (XANES) to study the local environment in metakaolin, which became a subject of significant debate, particularly regarding to the aluminum coordination environment determination [49,50].

Finally, we have recently presented two studies that engaged the complement XANES (local) and XRD-Rietveld (extended) characterization of model kaolinite and bentonite clays and its relevant heating products. These include kaolinite, metakaolinite, the SAS phase and mullite for the first study [48], and the bentonite and its corresponding metabentonite [51] . In this, the characteristic Al K-edge XANES spectra were obtained and discussed in terms of the crystalline thermal phase transformations and reported crystalline structures. We will remark that XANES is a spectroscopy widely used since the mid-1980s, because it is a powerful and versatile technique for obtaining information about the local atomic environment in materials and can be used to investigate specific elements in solids, liquids, gases or plasma [52,53].

The principal objective of the present work consists of the characterization of a set of complex aluminosilicates of technological interest, in the halloysite-mullite series, by means of X-ray based techniques (XRD and Al K-edge XANES), particularly in the Aluminum K-edge. This halloysite-mullite series is obtained by controlled calcination of high purity tubular halloysite clay. The study is complemented with a usual thermal analysis accompanied by microstructural observations made by scanning electron microscopy. As mentioned in many of the proposed applications a thermal treatment is proposed for the clay, within the explored temperature range.

Thinking about the low crystalline nature of some intermediates and products of the mentioned reactions, particularly HK, SAS and G, XANES arises to be an adequate technique for characterizing

these particular phases from the local point of view complementing the XRD-Rietveld analysis that evaluates the long distance order of those phases. A pure acid washed kaolinite and a sintered crystalline mullite (pure) and other reference aluminum containing materials are also evaluated for comparison. We suggest that these results will enlighten the design strategies of materials and technologies based in this nano clay.

2. Experimental procedures
2.1. The studied material

A commercial high purity halloysite ($Al_2Si_2O_5(OH)_4.2H_2O$) (Sigma Aldhrich; CAS Number 1332-58-7) was studied. The main properties of the studied nano clay can be summarized according to standard characterizations, *i.e.* molecular weight, diameter, refractive index, density, etc. (Table 1).

Table 1: Properties of the studied halloysite.

Molecular Weight	294.19 g/mol
Diameter range	30-70 nm
Length ranges	1-3 (µm)
Color	75-96, Hunter Brightness
Refractive index	n20/D 1.54
Pore size	1.26-1.34 mL/g
Surface area	64 m^2/g
Capacity (cation exchange capacity)	8.0 meq/g
Density	2.53 g/cm^3
pH	4.5 - 7.0

2.2. Heating halloysite clay conditions

The as received halloysite (Hallo-0) was heated in porcelain crucibles up to certain key temperatures with 10 °C/min heating rate and 30 minutes dwelling, in electric furnace, employing air atmosphere. Samples were labeled Hallo-i, where i was the respective maximum heating temperature. The key temperatures were chosen in order to ensure the mentioned phase transformations were completed (500, 800, 1100 and 1250 °C; labeled as Hallo-500, Hallo-800, Hallo-1100 and Hallo-1250, respectively).

5

2.3. DTA-TG, SEM and XRD experiments conditions

The effect of heat treatment was evaluated by simultaneous thermogravimetric and differential thermal analysis (DTA-TG) carried out on a Rigaku Evo Plus II equipment with 10°C/min heating rate using Pt crucibles in air atmosphere. Final batch firing conditions were obtained after this analysis (Table 2).

The evolution of the particle size and morphology of the clay and its fired products were examined by scanning electron microscopy SEM (Fei Quanta 200). Gold coated powders over carbon tape were analyzed in ultra-high vacuum conditions and 20.0 kV. An ETD detector was employed in back-scattered electron mode.

Identification of crystalline phases in the clay and fired materials were carried out by X-ray diffraction (XRD) (Philips 3020 with Cu-Kα radiation, Ni filter, at 40 kV-30 mA); with 0.04° and 2 seconds steps in the 3-70° range.

2.4. XANES experiments conditions

XANES experiments were performed in the Soft X-rays Spectroscopy (SXS) beamline of the Brazilian Synchrotron Light Laboratory (LNLS, Campinas, SP, Brazil). The beam focalization was performed using a Ni mirror. For Al K-edge, the monochromator employed was YB66, with a resolution of about 2 eV with a slit aperture of 2 mm. The I_0 incident photon flux intensity was measured using a mesh of Au located before the main chamber. The photon energies were calibrated using an Al metallic foil and setting the first inflection point to the energy of the K-edge of Al^0 at 1559 eV. The spectra were acquired at room temperature and the pressure chamber was about 10^{-4} torr in Fluorescence Mode. The aluminosilicate minerals were ground into fine powder (standard mesh # 200), and the powder samples were pressed uniformly on electric carbon tape supported on a stainless-steel sample holder for XANES measurements. All spectra were processed by standard methods from I_f/I_0 signal analysis, where I_f is the detected fluorescence intensity. The pre-edge region and the normalization background were realized by *Athena* [54]. The analyzed spectra were compared with an industrial high purity kaolinite (Fischer, Georgia, USA) and a sintered mullite (95% pure) and the fired corresponding intermediates presented elsewhere [48].

3. Results and discussions

3.1. Thermal analysis (TG, dTG and DTA)

The typical two mass losses can be observed in the 0-1300 °C range in the studied clay (TG). The first one (≈4%), observed below 150 °C, corresponds to the surface water loss. The second mass loss (≈12%) can be associated to the halloysite decomposition (dehydroxylation) into MH and also a water loss (equation 1). This analysis permits to identify the transformation temperature. No other mass loss (or gain) process occurs in this temperature range (Figure 1). In the third graph the DTA curve is plotted, and both endothermic and exothermic processes can be detected. The surface water loss presents two endothermic processes, centered at 72°C and 164 °C, in the DTG curve the first peak can be observed as two processes. A broad endothermic band centered at 505 °C, due to clay dehydroxylation reaction (equation 1) that is overlapped with α-β quartz

transformation with less energy involved, is the most important peak of the DTA analysis. The observed temperatures correspond to the TG ones and the previously reported ones [36,55]. An exothermic peak can be observed centered at 986 °C, this peak corresponds to the metahalloysite (MH) transformation into a spinel type aluminosilicate (SAS) and the mentioned mullite formation (equations 2 and 3). At higher temperatures the mullite formation processes (equation 4) were not observed, perhaps the amount of heat is too small for the equipment precision [56] and so, the XRD identification becomes necessary. The detected temperatures correspond to the ones observed for similar materials [41,42,55,57].

Transformation(1-4) illustrate these successive processes detected by TG-DTA. The simultaneous thermal analysis perm itted the determination of the actual temperature transformations. Based on TG-DTA information four materials were obtained after four thermal treatments that illustrate, together with the dried sample, the steps of this process.

The neighboring alumina and silica layers, and their water of hydration, create a packing disorder causing them to curve and roll up, forming multilayer tubes. The reason why flat kaolinite rolls into halloysite tubules, remains unclear. When the number of water molecules in the halloysite formula is two ($n = 2$), the clay is in the form of hydrated "halloysite-10 Å" with one layer of water molecules between multilayers. The "10 Å" designation indicates the spacing in the multilayer walls as the kaolinite plates roll up into a multiwalled cylinder. For $n = 0$, the structure is dehydrated "halloysite-7 Å" which may be obtained through an irreversible phase transition with loss of adsorbed water as the halloysite is heated to 90-150 °C. Afterwards "halloysite" has an endothermic peak at 500-600 °C due to structural dehydroxylation (metahalloysite formation) and then it remains stable until approximately 1000 °C. There are between 15-30 aluminosilicate layers rolled in the multilayer tubule walls with a layer spacing of 0.72 nm for the dehydrated halloysite.
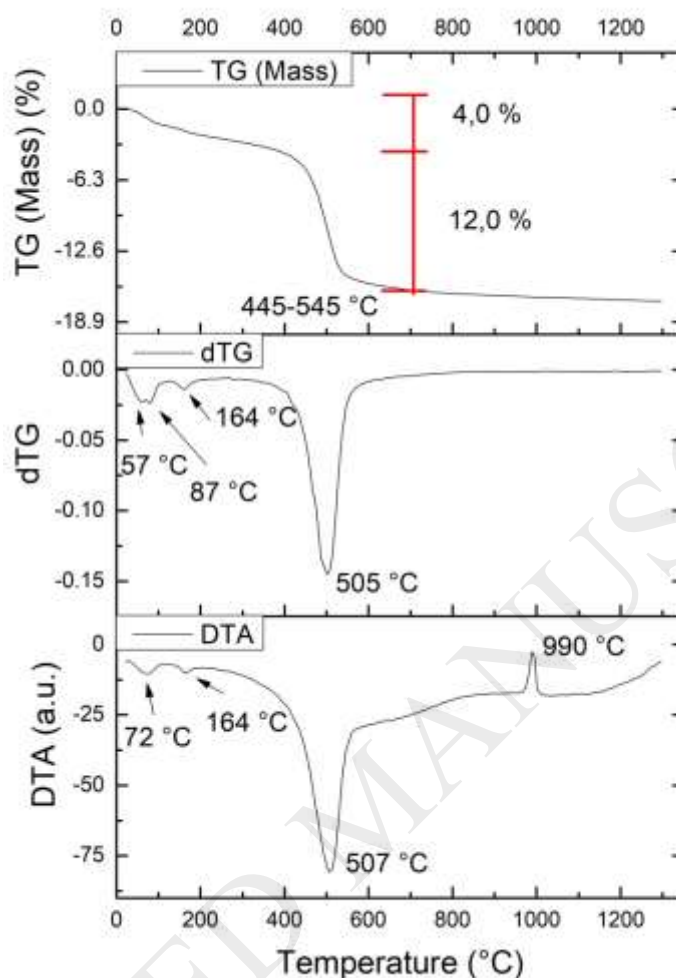
Figure 1: Thermal behavior of the studied Halloysite (hallo-0) TG, dTG and DTA

3.2. Mineralogical XRD analysis

By XRD analysis the halloysite structure was confirmed (Figure 2), particularly the so called "halloysite-7 Å". In the as received sample halloysite reflections are accompanied by quartz, traces of impurities. The impurities correspond to alunite and potash aluminate.

The XRD patterns of the heated clay can be observed as well. The different phase transitions (equations 1-4) can be clearly observed. This might be explained by a mild thermal treatment of the commercial nano clay performed by the supplier. The present phases were identified for the different heating temperatures (Table 2). The observed reflections correspond to disordered kaolinite reflections [58], and to confirm the presence of halloysite, in this case, a visual SEM based identification was needed. An important difference to highlight is that the intensity of the amorphous (silica rich) band centered at 22,5° can be observed, and this band was not observed in the heated kaolinite [48], and could be understood as an important difference between these two clays. After 1100 °C treatment, three small bands corresponding to the spinel type silicoaluminate

8

were clearly observed [41,42,59]. The nanocrystalline nature of this phase makes it sometimes difficult to observe by common XRD characterizations, and a proper structural characterization of this particular phase is interesting, due to this XRD analysis difficulty. Quartz was observed in the as received clay and the heating products (up to 1100°). The Hallo-1250 sample presented an important amount of cristobalite.

Table 2: Labels, identified phases. and PDF cards.

Sample	Heating temp. (°C)	Quartz (SiO_2)	Halloysite - 7 Å	SAS Spinel	Mullite ($3Al_2O_3.2SiO_2$)	Cristobalite (SiO_2)	Glassy Phase
PDF:		01-085-0797	00-029-1487	[60,61]	00-015-0776	01-082-0512	Band
Hallo-0	As received	X	x				
Hallo-500	500	X	x				x
Hallo-800	800	X					X
Hallo-1100	1100	X		x	x	x	X
Hallo-1250	1250	X			x	x	X

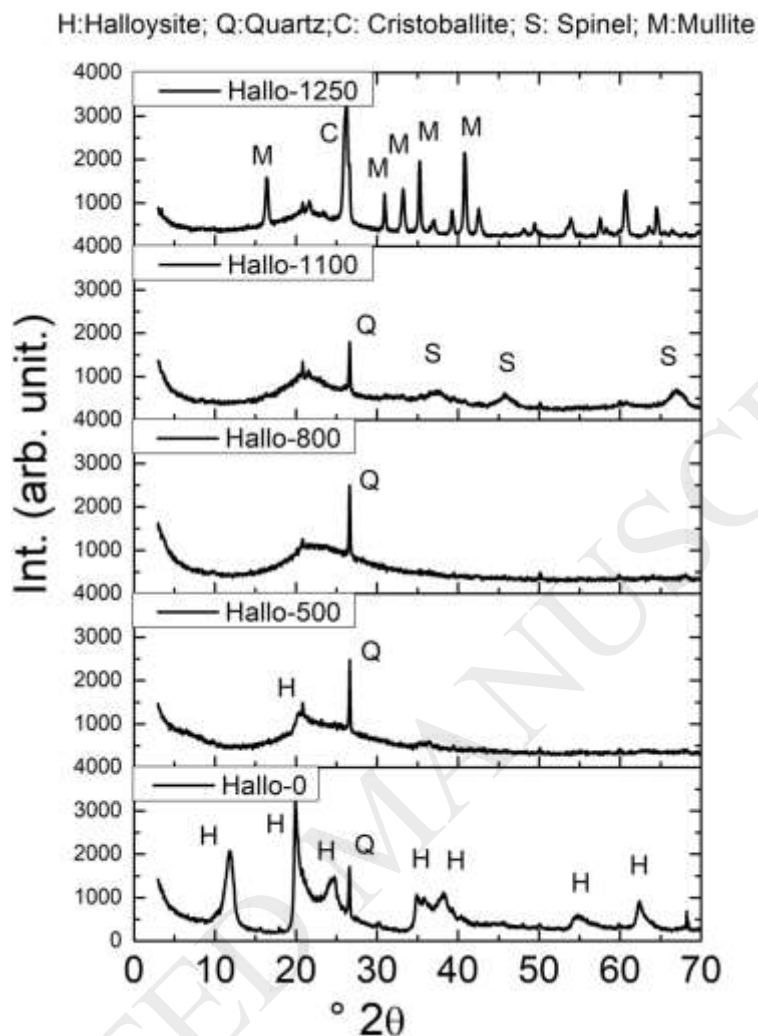H:Halloysite; Q:Quartz;C: Cristoballite; S: Spinel; M:Mullite

Figure 2: XRD patterns of the studied Halloysite and the heated samples; principal reflections are labeled. Matched phases are shown in table 2.

3.3. *SEM analysis*

One halloysite predominant form is a hollow tubular structure in the sub-micrometer range. The size of halloysite tubules varies from 500-1000 nm in length and 15-100 nm in inner diameter depending on the deposit [32,33,62,17,19,63], which was confirmed for the studied sample (Figure 3). The analyzed agglomerate was 50 μm, the border of the agglomerate was focused in order to have high contrast between the clay and the carbon connecting tape employed as sample holder.

The microscopy SEM show that both the halloysite and its calcining products have a needle-tubular morphology, where sizes and length/diameter ratios previously reported were confirmed (Figure 4). The quartz presence was also observed as not acicular coarse grains. After high temperature treatments (1100 and 1250 °C) the needle shape is retained, especially in these not

10

pressed samples. However, the principal aim of this work was to assess the chemical changes at an atomic local scale by the X ray absorptions analysis shown in the next section.
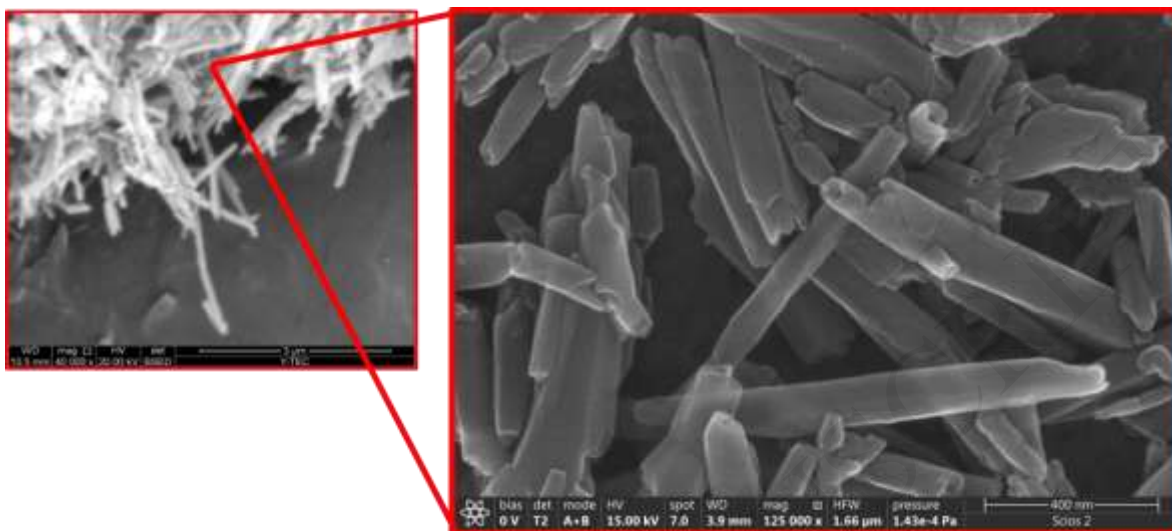

Figure 3: SEM images of the studied as received clay (x40000 and x125000). Tubular shape can be easily observed in the observed agglomerate.

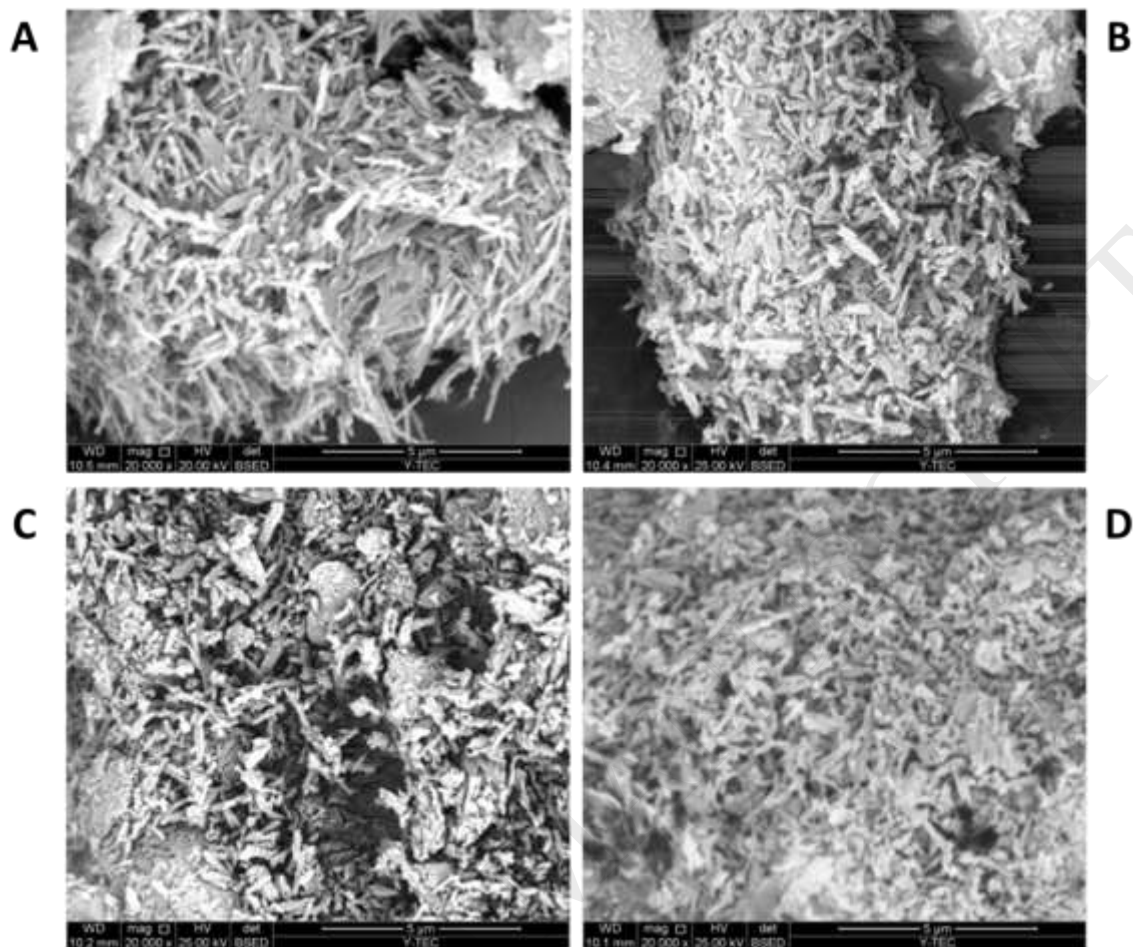**Figure 4: SEM images (x20000) of the Halloysite and the heated Halloysite (Hallo-0; Hallo-800; Hallo-1100; Hallo-1250, (A, B C and D respectively).**

3.4. *XANES analysis*

The XANES spectra of the halloysite and its corresponding thermal products (full black line) were compared to the kaolinite XANES spectra and its fired products (full dark gray line), and mullite (full light grey line) (Figure 5).
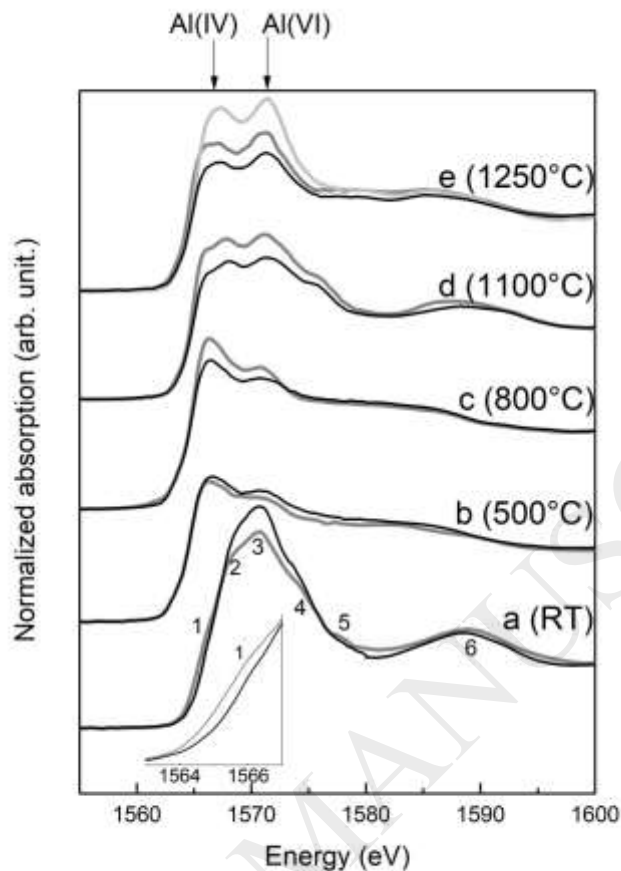
Figure 5: Al K-XANES spectra of the Halloysite and its corresponding thermal products (full black line) compared to the Kaolinite XANES spectra, its corresponding thermal products (gray line + empty spot) and Mullite (full gray line).

Following the assignment made by Dien Li *et al.* [64] the shoulder (1) at 1565.8 eV is related to a pre-edge feature associated to 1s→a_{1g} (3s-like) electronic transition, or dipole-forbidden transition of Al 1s electrons to anti-bonding a_{1g} (3s-like) states. This forbidden peak appears because the distortion of the coordination octahedra permits a mixture of Al s and p states. Ph. Ildefonse *et al*. [38] attributes shoulder (1) to the overlap of the feature of Al(IV) and the Al(VI) in a highly ordered kaolinite. The assignments made by Li *et al*. (1995) are compatible with those made by Ph. Ildefonse *et al*. (1994) according to the interpretation in which the systems without center of symmetry give rise to transitions not allowed by rules of Laporte [65]. The peak labeled as (2) is associated with allowed transition of Al 1s electrons to the anti- bonding t_{1u} states, 1s→t_{1u} (3p-like) transition, and it is located at 1568.0 eV. The peak (3), at 1570.4 eV, is identified with a multiple scattering resonance. The peak labeled as (4) represents the forbidden 1s→t_{2g} (3d-like) transition and it is at 1573.2 eV, while the resonances marked as (5) and (6) are identified with multiple scattering and forbidden 1s→e_g (3d-like) transition, at 1579.0 eV and 1589.5 eV, respectively.

13

Two important characteristics are observed in the XANES spectra. The first is the much lower intensity of the shoulder (1) for the halloysite with respect to the intensity of such shoulder for the kaolinite (see inside graph in Figure 5). This is compatible with what was published by Ph. Ildefonse *et al*. (1994) for model compounds with Al(VI) coordinated to oxygen in a dioctahedral layer, particularly in the comparison between poorly ordered kaolinite and halloysite. According to the language of group theory, halloysite presents environments more centrosymmetric than kaolinite [65].

The second feature is the lower intensity for kaolinite compared to halloysite in the region between 1560 and 1580 eV. The shape of the XANES directly reflects the excited state electronic densities of states in a material [66], or, in other words, the near edge structure can be interpreted in terms of unoccupied levels with a majority contribution of p and d states [67]. The density of unoccupied states has a crucial preponderance in the form and intensity of the XANES spectra. Although kaolinite and halloysite have the same formal stoichiometric structure, $Al_2Si_2O_5(OH)_4$, the difference in intensities can be interpreted, not as a change in morphological structure, but as a greater number of unoccupied electronic states in halloysite.

Therefore, these two facts, greater center symmetry in Al environments and higher density of unoccupied p-states for halloysite with respect to kaolinite, allow to observe differences that must be studied to determine their origin. These studies involve *ab-initio* calculations and DFT calculations that are outside the scope of this paper.

For thermal treatment at 500 °C, the same XANES structure is observed in both cases. That is, the local environments of Al in thermally treated Hallo-500 have the same structure as MK. In a recent paper [48] the main characteristics of the Al K XANES spectra for MK were published. In addition, a systematic and detailed study of the local structure of aluminum in MK can be found in the works of White *et al* [68–70], and Al(III), Al(V) and Al(VI) coordination were identified for metahalloysite [49,50,72,73].

For heat treatment at 800 °C, it is observed a higher intensity for the resonances assigned to the sites Al(IV) and Al(VI) for Kaol-800 than for Hallo-800. These differences in intensities continue to manifest for the following thermal treatments. For example, for 1100 °C the characteristics of the spectrum are the same but the intensities are different, in the same way as in the case of mullite.

XANES spectroscopy of solids involves complicated processes (transition probabilities, full multiple scattering, etc). The peak for Al(IV) is assigned to the allowed transition of Al 1s electrons to the antibonding t_2 (3p-like) states, and the peak for Al(VI) is assigned to the allowed transition of Al 1s electrons to the antibonding t_{1u} (3p-like) states [64].

According to the calculation method for Al(IV)/Al(VI) presented by Kato et al. [74], was obtained that Al(IV)/Al(VI) $\cong$ 0.6, which allows to conclude that the number of tetrahedral sites with respect to the octahedral sites for the three samples (Hallo-1100, Hallo-1250 and mullite) is the same. This means that although the relative amounts of Al sites are constant, electronic interactions of aluminum with its environment are different. In other words, for the mullite there are more *3p*-holes available than for the Kaol-1250 and Hallo-1250, according to the intensity of the transitions. This is the distinctive quality provided by the XANES technique: the relation Al(IV)/Al(VI) is approximately the same for the three samples but the electronic interaction is significantly different. The results obtained here for Hallo-1250 for the relationship Al(IV)/Al(VI) are in

14

accordance with what was reported by the pioneer work of Mackenzie et al. and Schneider et al. [45,57].

4. Conclusions

Halloysite thermal processes present local and long distance order nature. The extended and local range order structure characterization of commercial halloysite clay and its calcination products was carried out by means of two X-ray based techniques: XRD and XANES, respectively. In order to give context to these characterizations, thermal analyses (TG-DTA) and SEM were carried out.

Both crystalline and low crystallinity phases were described after thermal transformations in the studied material: halloysite, metahalloysite, the spinel type aluminosilicate SAS and mullite.

The tubular morphology was retained after thermal treatments. The not crystalline structure of the tubular metahalloysite fired at 800 °C presents potential applications. The 1100 °C fired samples presented the spinel aluminosilicate phase, this was identified by XRD and, acicular morphology was confirmed, showing a solid state transformation. Finally, after high temperature treatments the mullite phase was detected as the only aluminum containing crystalline phase accompanied by cristobalite and glassy phase.

The studied clay mineral presented a clear behavior and allows us to identify the proper thermal treatments in order to achieve the complete transformation of the material.

Al atoms in the different materials were locally described by Al K XANES, and compared with the kaolinite and its fired product or sintered mullite. Both coordination geometries and first neighbors were established in each phase and consistently compared with further studies on aluminum oxides and minerals. Al has octahedral coordination in halloysite as observed in kaolinite, and Al(III), Al(V) and Al(VI) coordination were identified for meta-halloysite. Finally, Al(VI) and Al(VI) were found in the spinel type aluminosilicate and mullite. In addition, it was established that the Al(IV)/Al(VI) ratio is the same for the three samples (Hallo-1100, Hallo-1250 and mullite).

5. Acknowledgments

6. References

[1]   S.W. Bailey, Halloysite- a critical assessment., Sci. Geol.-Memoires. 86 (1990) 89–98.

[2]   S.L. Johnson, Thermal Stability of Halloysite by High-Pressure Differential Thermal Analysis, Clays Clay Miner. 38 (1990) 477–484. doi:10.1346/CCMN.1990.0380503.

[3]   S.L. West, G.N. White, Y. Deng, K.J. McInnes, A.S.R. Juo, J.B. Dixon, Kaolinite, Halloysite, and Iron Oxide Influence on Physical Behavior of Formulated Soils, Soil Sci. Soc. Am. J. 68 (2004) 1452–1460. doi:10.2136/sssaj2004.1452.

[4]   G.J. Churchman, P. Pasbakhsh, S. Hillier, The rise and rise of halloysite, Clay Miner. 51 (2016) 303–308. doi:10.1180/claymin.2016.051.3.00.

[5]   S. Hillier, R. Brydson, E. Delbos, T. Fraser, N. Gray, H. Pendlowski, I. Phillips, J. Robertson, I. Wilson, Correlations among the mineralogical and physical properties of halloysite nanotubes (HNTs), Clay Miner. 51 (2016) 325–350. doi:10.1180/claymin.2016.051.3.11.

[6]   E. Joussein, Chapter 2 - Geology and Mineralogy of Nanosized Tubular Halloysite, in: P. Yuan, A. Thill, F. Bergaya (Eds.), Dev. Clay Sci., Elsevier, 2016: pp. 12–48. doi:10.1016/B978-0-08-100293-3.00002-9.

[7]   K. Nagasawa, H. Noro, Mineralogical properties of halloysites of weathering origin, Chem. Geol. 60 (1987) 145–149. doi:10.1016/0009-2541(87)90120-3.

[8]   P. Quantin, J. Gautheyrou, P. Lorenzoni, Halloysite formation through in situ weathering of volcanic glass from trachytic pumices, Vico's volcano, Italy, Clay Miner. 23 (1988) 423–437.

[9]   S.W. Bailey, Halloysite - a critical assessment, Sci. Geol. - Memoire. 86 (1990) 89–98.

[10]   M. Soma, G.J. Churchman, B.K.G. Theng, X-ray photoelectron spectroscopic analysis of halloysites with different composition and particle morphology, Clay Miner. 27 (1992) 413–421.

[11]   P. Yuan, P.D. Southon, Z. Liu, M.E.R. Green, J.M. Hook, S.J. Antill, C.J. Kepert, Functionalization of Halloysite Clay Nanotubes by Grafting with γ-Aminopropyltriethoxysilane, J. Phys. Chem. C. 112 (2008) 15742–15751. doi:10.1021/jp805657t.

[12]   F. Cravero, L. Fernández, S. Marfil, M. Sanchez, P. Maiza, A. Martinez, Spheroidal halloysites from Patagonia, Argentina: Some aspects of their formation and applications, Appl. Clay Sci. 131 (2016) 48–58.

[13]   M. Massaro, G. Cavallaro, C.G. Colletti, G. Lazzara, S. Milioto, R. Noto, S. Riela, Chemical modification of halloysite nanotubes for controlled loading and release, J. Mater. Chem. B. 6 (2018) 3415–3433. doi:10.1039/C8TB00543E.

[14]   G.B. Mitra, Spiral structure of 7 Å halloysite: mathematical models, Clays Clay Miner. 61 (2013) 499–507.

[15]   D.G. Shchukin, G.B. Sukhorukov, R.R. Price, Y.M. Lvov, Halloysite Nanotubes as Biomimetic Nanoreactors, Small. 1 (2005) 510–513. doi:10.1002/smll.200400120.

[16]   Y.M. Lvov, D.G. Shchukin, H. Mohwald, R.R. Price, Halloysite clay nanotubes for controlled release of protective agents, ACS Nano. 2 (2008) 814–820.

[17]   M. Du, B. Guo, D. Jia, Newly emerging applications of halloysite nanotubes: a review, Polym. Int. 59 (2010) 574–582. doi:10.1002/pi.2754.

[18]   R. Kamble, M. Ghag, S. Gaikawad, B.K. Panda, Halloysite Nanotubes and Applications: A Review., J. Adv. Sci. Res. 3 (2012).

[19]   D. Rawtani, Y.K. Agrawal, Multifarious applications of halloysite nanotubes: a review, Rev Adv Mater Sci. 30 (2012) 282–295.

[20]   R.S. Hebbar, A.M. Isloor, K. Ananda, A.F. Ismail, Fabrication of polydopamine functionalized halloysite nanotube/polyetherimide membranes for heavy metal removal, J. Mater. Chem. A. 4 (2016) 764–774.

[21]   Y. Lvov, W. Wang, L. Zhang, R. Fakhrullin, Halloysite clay nanotubes for loading and sustained release of functional compounds, Adv. Mater. 28 (2016) 1227–1250.

[22]   E. Joussein, S. Petit, J. Churchman, B. Theng, D. Righi, B. Delvaux, Halloysite clay minerals – a review, Clay Miner. 40 (2005) 383–426. doi:10.1180/0009855054040180.

[23]   V. Vergaro, E. Abdullayev, Y.M. Lvov, A. Zeitoun, R. Cingolani, R. Rinaldi, S. Leporatti, Cytocompatibility and uptake of halloysite clay nanotubes, Biomacromolecules. 11 (2010) 820–826.

[24]   G.J. Churchman, P. Pasbakhsh, S. Hillier, The rise and rise of halloysite, Clay Miner. 51 (2016) 303–308.

[25]   F. Cravero, L. Fernández, S. Marfil, M. Sánchez, P. Maiza, A. Martínez, Spheroidal halloysites from Patagonia, Argentina: Some aspects of their formation and applications, Appl. Clay Sci. 131 (2016) 48–58. doi:10.1016/j.clay.2016.01.011.

[26] P.C. Ryan, F.J. Huertas, F.W.C. Hobbs, L.N. Pincus, Kaolinite and halloysite derived from sequential transformation of pedogenic smectite and kaolinite-smectite in a 120 ka tropical soil chronosequence, Clays Clay Miner. 64 (2016) 639–667.

[27] N.G. Veerabadran, R.R. Price, Y.M. Lvov, Clay nanotubes for encapsulation and sustained release of drugs, Nano. 02 (2007) 115–120. doi:10.1142/S1793292007000441.

[28] P. Yuan, P.D. Southon, Z. Liu, M.E. Green, J.M. Hook, S.J. Antill, C.J. Kepert, Functionalization of halloysite clay nanotubes by grafting with γ-aminopropyltriethoxysilane, J. Phys. Chem. C. 112 (2008) 15742–15751.

[29] R. Kamble, M. Ghag, S. Gaikawad, B.K. Panda, Halloysite Nanotubes and Applications: A Review., J. Adv. Sci. Res. 3 (2012).

[30] B. Szczepanik, P. Słomkiewicz, M. Garnuszek, P. Rogala, D. BanaŚ, K.-K. Aldona, I. Stabrawa, Effect of temperature on halloysite acid treatment for efficient chloroaniline removal from aqueous solutions, Clays Clay Miner. 65 (2017) 155–167.

[31] R.L. Frost, J. Kristof, Intercalation of halloysite: A raman spectroscopic study, Clays Clay Miner. 45 (1997) 551–563.

[32] G.J. Churchman, T.J. Davy, L.A.G. Aylmore, R.J. Gilkes, P.G. Self, Characteristics of fine pores in some halloysites, Clay Miner. 30 (1995) 89–98.

[33] B. Singh, R.J. Gilkes, An electron optical investigation of the alteration of kaolinite to halloysite, Clays Clay Miner. 40 (1992) 212–229.

[34] G.W. Brindley, M. Nakahira, Kinetics of Dehydroxylation of Kaolinite and Halloysite, J. Am. Ceram. Soc. 40 (1957) 346–350. doi:10.1111/j.1151-2916.1957.tb12549.x.

[35] G.W. Brindley, M. Nakahira, The Kaolinite-Mullite Reaction Series: II, Metakaolin, J. Am. Ceram. Soc. 42 (1959) 314–318. doi:10.1111/j.1151-2916.1959.tb14315.x.

[36] A.K. Chakraborty, Phase transformation of kaolinite clay, Springer, 2016.

[37] De Aza, X. Turrillas, M.A. Rodriguez, T. Duran, P. Pena, Time-resolved powder neutron diffraction study of the phase transformation sequence of kaolinite to mullite, J. Eur. Ceram. Soc. 34 (2014) 1409–1421. doi:10.1016/j.jeurceramsoc.2013.10.034.

[38] P. Ildefonse, R.J. Kirkpatrick, B. Montez, G. Calas, A.M. Flank, P. Lagarde, 27a1 mas nmr and aluminum x-ray absorption near edge structure study of imogolite and allophanes, Clays Clay Miner. 42 (1994) 276–287. doi:https://doi.org/10.1346/CCMN.1994.0420306.

[39] Y.-F. Chen, M.-C. Wang, M.-H. Hon, Phase transformation and growth of mullite in kaolin ceramics, J. Eur. Ceram. Soc. 24 (2004) 2389–2397.

[40] A.K. Chakraborty, Crystallization Studies of Preheated Metakaolinite, in: Phase Transform. Kaolinite Clay, Springer, New Delhi, 2014: pp. 109–114. doi:10.1007/978-81-322-1154-9_11.

[41] K. Okada, N. ŌTsuka, J. Ossaka, Characterization of Spinel Phase Formed in the Kaolin-Mullite Thermal Sequence, J. Am. Ceram. Soc. 69 (1986).

[42] J. Sanz, A. Madani, J.M. Serratosa, J.S. Moya, S. Aza, Aluminum-27 and Silicon-29 Magic-Angle Spinning Nuclear Magnetic Resonance Study of the Kaolinite-Mullite Transformation, J. Am. Ceram. Soc. 71 (1988).

[43] M. Bellotto, A. Gualtieri, G. Artioli, S.M. Clark, Kinetic study of the kaolinite-mullite reaction sequence. Part I: Kaolinite dehydroxylation, Phys. Chem. Miner. 22 (1995) 207–217. doi:10.1007/BF00202253.

[44] A. Gualtieri, M. Bellotto, G. Artioli, S.M. Clark, Kinetic study of the kaolinite-mullite reaction sequence. Part II: Mullite formation, Phys. Chem. Miner. 22 (1995) 215–222. doi:10.1007/BF00202254.

[45] H. Schneider, J. Schreuer, B. Hildmann, Structure and properties of mullite—A review, J. Eur. Ceram. Soc. 28 (2008) 329–344. doi:10.1016/j.jeurceramsoc.2007.03.017.

[46] M.F. Serra, M.S. Conconi, G. Suarez, E.F. Agietti, N.M. Rendtorff, Firing transformations of an argentinean calcareous commercial clay, Cerâmica. 59 (2013) 254–261. doi:10.1590/S0366-69132013000200010.

[47] M.S. Conconi, M.R. Gauna, M.F. Serra, G. Suarez, E.F. Aglietti, N.M. Rendtorff, Quantitative firing transformations of a triaxial ceramic by X-ray diffraction methods, Cerâmica. 60 (2014) 524–531. doi:10.1590/S0366-69132014000400010.

[48] L. Andrini, M.R. Gauna, M.S. Conconi, G. Suarez, F.G. Requejo, E.F. Aglietti, N.M. Rendtorff, Extended and local structural description of a kaolinitic clay, its fired ceramics and intermediates: An XRD and XANES analysis, Appl. Clay Sci. 124–125 (2016) 39–45. doi:10.1016/j.clay.2016.01.049.

[49] C.E. White, L.M. Perander, J.L. Provis, J.S.J. van Deventer, The use of XANES to clarify issues related to bonding environments in metakaolin: a discussion of the paper S. Sperinck et al., "Dehydroxylation of kaolinite to metakaolin-a molecular dynamics study," J. Mater. Chem., 2011, 21, 2118–2125, J. Mater. Chem. 21 (2011) 7007–7010. doi:10.1039/C1JM10379B.

[50] C.E. White, J.L. Provis, D.P. Riley, T. Proffen, L.M. Perander, D. Van, Characterisation and description of the structure of metakaolin by total scattering, density functional theory, and X-ray spectroscopy, in: Concr. Repair Rehabil. Retrofit. III - Proc. 3rd Int. Conf. Concr. Repair Rehabil. Retrofit., Alexander, M. G., Beushausen, H. D., Dehn, F., Moyo, P. (Eds.), CRC Press, Cape Town, South Africa, 2012: pp. 1426–1432. https://books.google.com.ar/books?hl=es&lr=&id=nwbNBQAAQBAJ&oi=fnd&pg=PP1&dq=%22Characterisation+and+description+of+the+structure+of+metakaolin+by+total+scattering,+density+functional+theory,+and+X-ray+spectroscopy%22&ots=kFgycYUwQb&sig=Xq0vApIVbopT2YH12JmJkl7_IQQ#v=onepage&q=%22Characterisation%20and%20description%20of%20the%20structure%20of%20metakaolin%20by%20total%20scattering%2C%20density%20functional%20theory%2C%20and%20X-ray%20spectroscopy%22&f=false.

[51] L. Andrini, R.M. Toja, M.R. Gauna, M.S. Conconi, F.G. Requejo, N.M. Rendtorff, Extended and local structural characterization of a natural and 800 C fired Na-montmorillonite–Patagonian bentonite by XRD and Al/Si XANES, Appl. Clay Sci. 137 (2017) 233–240.

[52] D.C. Koningsberger, R. Prins, X-ray absorption: principles, applications, techniques of EXAFS, SEXAFS, and XANES, (1988).

[53] G. Bunker, Introduction to XAFS: A Practical Guide to X-ray Absorption Fine Structure Spectroscopy, Cambridge University Press, 2010.

[54] B. Ravel, M. Newville, ATHENA, ARTEMIS, HEPHAESTUS: data analysis for X-ray absorption spectroscopy using IFEFFIT, J. Synchrotron Radiat. 12 (2005) 537–541.

[55] C. Duce, S.V. Ciprioti, L. Ghezzi, V. Ierardi, M.R. Tinè, Thermal behavior study of pristine and modified halloysite nanotubes, J. Therm. Anal. Calorim. 121 (2015) 1011–1019. doi:10.1007/s10973-015-4741-7.

[56] V. Viswabaskaran, F.D. Gnanam, M. Balasubramanian, Mullitisation behaviour of calcined clay–alumina mixtures, Ceram. Int. 29 (2003) 561–571. doi:10.1016/S0272-8842(02)00203-1.

[57] K.J.D. MacKenzie, R.H. Meinhold, I.W.M. Brown, G.V. White, The formation of mullite from kaolinite under various reaction atmospheres, J. Eur. Ceram. Soc. 16 (1996) 115–119. doi:10.1016/0955-2219(95)00143-3.

[58] L. Riber, H. Dypvik, R. Sørlie, R.E. Ferrell Jr, Clay minerals in deeply buried paleoregolith profiles, Norwegian North Sea, Clays Clay Miner. 64 (2016) 588–607.

[59] M.E. Ouahabi, L. Daoudi, F. Hatert, N. Fagel, Modified Mineral Phases During Clay Ceramic Firing, Clays Clay Miner. 63 (2015) 404–413.

[60] K. Okada, N. ŌTsuka, J. Ossaka, Characterization of Spinel Phase Formed in the Kaolin-Mullite Thermal Sequence, J. Am. Ceram. Soc. 69 (1986) C–251. doi:10.1111/j.1151-2916.1986.tb07353.x.

[61] J. Sanz, A. Madani, J.M. Serratosa, J.S. Moya, S. Aza, Aluminum-27 and Silicon-29 Magic-Angle Spinning Nuclear Magnetic Resonance Study of the Kaolinite-Mullite Transformation, J. Am. Ceram. Soc. 71 (1988) C418–C421. doi:10.1111/j.1151-2916.1988.tb07513.x.

[62] E. Joussein, S. Petit, J. Churchman, B. Theng, D. Righi, B. Delvaux, Halloysite clay minerals–a review, De Gruyter, 2005.

[63] E. Joussein, Chapter 2 - Geology and Mineralogy of Nanosized Tubular Halloysite, in: P. Yuan, A. Thill, F. Bergaya (Eds.), Dev. Clay Sci., Elsevier, 2016: pp. 12–48. doi:10.1016/B978-0-08-100293-3.00002-9.

[64] D. Li, G.M. Bancroft, M.E. Fleet, X.H. Feng, Y. Pan, Al K-edge XANES spectra of aluminosilicate minerals, Mineralogical Society of America, 1995.

[65] T. Yamamoto, Assignment of pre-edge peaks in K-edge x-ray absorption spectra of 3d transition metal compounds: electric dipole or quadrupole?, X-Ray Spectrom. 37 (2008) 572–584.

[66] J.J. Rehr, A.L. Ankudinov, Progress in the theory and interpretation of XANES, Coord. Chem. Rev. 249 (2005) 131–140.

[67] E. Tamura, J. Van Ek, M. Fröba, J. Wong, X-Ray absorption near edge structure in metals: relativistic effects and core-hole screening, Phys. Rev. Lett. 74 (1995) 4899.

[68] C.E. White, L.M. Perander, J.L. Provis, D. Van, The use of XANES to clarify issues related to bonding environments in metakaolin: A discussion of the paper S. Sperinck et al., "dehydroxylation of kaolinite to metakaolin-a molecular dynamics study," J. Mater. Chem., 2011, 21, 2118-2125, J. Mater. Chem. 21 (2011) 7007–7010. doi:10.1039/c1jm10379b.

[69] C.E. White, J.L. Provis, D.P. Riley, Th. Proffen, L.M. Perander, D. Van, Characterisation and description of the structure of metakaolin by total scattering, density functional theory, and X-ray spectroscopy, in: 2012: pp. 1426–1432.

[70] C.E. White, K. Page, N.J. Henson, J.L. Provis, In situ synchrotron X-ray pair distribution function analysis of the early stages of gel formation in metakaolin-based geopolymers, Appl. Clay Sci. 73 (2013) 17–25. doi:10.1016/j.clay.2012.09.009.

[71] C.E. White, J.L. Provis, T. Proffen, D.P. Riley, J.S.J. van Deventer, Density Functional Modeling of the Local Structure of Kaolinite Subjected to Thermal Dehydroxylation, J. Phys. Chem. A. 114 (2010) 4988–4996. doi:10.1021/jp911108d.

[72] C.E. White, K. Page, N.J. Henson, J.L. Provis, In situ synchrotron X-ray pair distribution function analysis of the early stages of gel formation in metakaolin-based geopolymers, Appl. Clay Sci. 73 (2013) 17–25. doi:10.1016/j.clay.2012.09.009.

[73] L. Andrini, M.R. Gauna, M.S. Conconi, G. Suarez, F.G. Requejo, E.F. Aglietti, N.M. Rendtorff, Extended and local structural description of a kaolinitic clay, its fired ceramics and intermediates: An XRD and XANES analysis, Appl. Clay Sci. 124–125 (2016) 39–45. doi:10.1016/j.clay.2016.01.049.

[74] Y. Kato, K. Shimizu, N. Matsushita, T. Yoshida, H. Yoshida, A. Satsuma, T. Hattori, Quantification of aluminium coordinations in alumina and silica–alumina by Al K-edge XANES, Phys. Chem. Chem. Phys. 3 (2001) 1925–1929. doi:10.1039/B100610J.

[2] S.L. Johnson, Thermal Stability of Halloysite by High-Pressure Differential Thermal Analysis, Clays Clay Miner. 38 (1990) 477–484. doi:10.1346/CCMN.1990.0380503.

[3]   S.L. West, G.N. White, Y. Deng, K.J. McInnes, A.S.R. Juo, J.B. Dixon, Kaolinite, Halloysite, and Iron Oxide Influence on Physical Behavior of Formulated Soils, Soil Sci. Soc. Am. J. 68 (2004) 1452–1460. doi:10.2136/sssaj2004.1452.

[4]   G.J. Churchman, P. Pasbakhsh, S. Hillier, The rise and rise of halloysite, Clay Miner. 51 (2016) 303–308. doi:10.1180/claymin.2016.051.3.00.

[5]   S. Hillier, R. Brydson, E. Delbos, T. Fraser, N. Gray, H. Pendlowski, I. Phillips, J. Robertson, I. Wilson, Correlations among the mineralogical and physical properties of halloysite nanotubes (HNTs), Clay Miner. 51 (2016) 325–350. doi:10.1180/claymin.2016.051.3.11.

[6]   E. Joussein, Chapter 2 - Geology and Mineralogy of Nanosized Tubular Halloysite, in: P. Yuan, A. Thill, F. Bergaya (Eds.), Dev. Clay Sci., Elsevier, 2016: pp. 12–48. doi:10.1016/B978-0-08-100293-3.00002-9.

[7]   K. Nagasawa, H. Noro, Mineralogical properties of halloysites of weathering origin, Chem. Geol. 60 (1987) 145–149. doi:10.1016/0009-2541(87)90120-3.

[8]   P. Quantin, J. Gautheyrou, P. Lorenzoni, Halloysite formation through in situ weathering of volcanic glass from trachytic pumices, Vico's volcano, Italy, Clay Miner. 23 (1988) 423–437.

[9]   S.W. Bailey, Halloysite - a critical assessment, Sci. Geol. - Memoire. 86 (1990) 89–98.

[10]   M. Soma, G.J. Churchman, B.K.G. Theng, X-ray photoelectron spectroscopic analysis of halloysites with different composition and particle morphology, Clay Miner. 27 (1992) 413–421.

[11]   P. Yuan, P.D. Southon, Z. Liu, M.E.R. Green, J.M. Hook, S.J. Antill, C.J. Kepert, Functionalization of Halloysite Clay Nanotubes by Grafting with γ-Aminopropyltriethoxysilane, J. Phys. Chem. C. 112 (2008) 15742–15751. doi:10.1021/jp805657t.

[12]   F. Cravero, L. Fernández, S. Marfil, M. Sanchez, P. Maiza, A. Martinez, Spheroidal halloysites from Patagonia, Argentina: Some aspects of their formation and applications, Appl. Clay Sci. 131 (2016) 48–58.

[13]   M. Massaro, G. Cavallaro, C.G. Colletti, G. Lazzara, S. Milioto, R. Noto, S. Riela, Chemical modification of halloysite nanotubes for controlled loading and release, J. Mater. Chem. B. 6 (2018) 3415–3433. doi:10.1039/C8TB00543E.

[14]   K. Nagasawa, H. Noro, Mineralogical properties of halloysites of weathering origin, Chem. Geol. 60 (1987) 145–149. doi:10.1016/0009-2541(87)90120-3.

[15]   P. Quantin, J. Gautheyrou, P. Lorenzoni, Halloysite formation through in situ weathering of volcanic glass from trachytic pumices, Vico's Volcano, Italy, Clay Miner. 23 (1988) 423–37.

[16]   M. Soma, G.J. Churchman, B.K.G. Iheng, X-ray photoelectron spectroscopic analysis of halloysites with different composition and particle morphology, Clay Miner. 27 (1992) 413–413.

[17]   P. Yuan, D. Tan, F. Aannabi-Bergaya, W. Yan, M. Fan, D. Liu, H. He, Changes in structure, morphology, porosity, and surface activity of mesoporous halloysite nanotubes under heating, Clays Clay Miner. 60 (2012) 561–573.

[18]   G.B. Mitra, Spiral structure of 7 Å halloysite: mathematical models, Clays Clay Miner. 61 (2013) 499–507.

[19]   D.G. Shchukin, G.B. Sukhorukov, R.R. Price, Y.M. Lvov, Halloysite Nanotubes as Biomimetic Nanoreactors, Small. 1 (2005) 510–513. doi:10.1002/smll.200400120.

[20]   Y.M. Lvov, D.G. Shchukin, H. Mohwald, R.R. Price, Halloysite clay nanotubes for controlled release of protective agents, ACS Nano. 2 (2008) 814–820.

[21]   M. Du, B. Guo, D. Jia, Newly emerging applications of halloysite nanotubes: a review, Polym. Int. 59 (2010) 574–582. doi:10.1002/pi.2754.

[22] R. Kamble, M. Ghag, S. Gaikawad, B.K. Panda, Halloysite Nanotubes and Applications: A Review., J. Adv. Sci. Res. 3 (2012).

[23] D. Rawtani, Y.K. Agrawal, Multifarious applications of halloysite nanotubes: a review, Rev Adv Mater Sci. 30 (2012) 282–295.

[24] R.S. Hebbar, A.M. Isloor, K. Ananda, A.F. Ismail, Fabrication of polydopamine functionalized halloysite nanotube/polyetherimide membranes for heavy metal removal, J. Mater. Chem. A. 4 (2016) 764–774.

[25] Y. Lvov, W. Wang, L. Zhang, R. Fakhrullin, Halloysite clay nanotubes for loading and sustained release of functional compounds, Adv. Mater. 28 (2016) 1227–1250.

[26] E. Joussein, S. Petit, J. Churchman, B. Theng, D. Righi, B. Delvaux, Halloysite clay minerals – a review, Clay Miner. 40 (2005) 383–426. doi:10.1180/0009855054040180.

[27] V. Vergaro, E. Abdullayev, Y.M. Lvov, A. Zeitoun, R. Cingolani, R. Rinaldi, S. Leporatti, Cytocompatibility and uptake of halloysite clay nanotubes, Biomacromolecules. 11 (2010) 820–826.

[28] E. Joussein, S. Petit, J. Churchman, B. Theng, D. Righi, B. Delvaux, Halloysite clay minerals–a review, De Gruyter, 2005.

[29] G.J. Churchman, T.J. Davy, L.A.G. Aylmore, R.J. Gilkes, P.G. Self, Characteristics of fine pores in some halloysites, Clay Miner. 30 (1995) 89–98.

[30] P.C. Ryan, F.J. Huertas, F.W.C. Hobbs, L.N. Pincus, Kaolinite and halloysite derived from sequential transformation of pedogenic smectite and kaolinite-smectite in a 120 ka tropical soil chronosequence, Clays Clay Miner. 64 (2016) 639–667.

[31] N.G. Veerabadran, R.R. Price, Y.M. Lvov, Clay nanotubes for encapsulation and sustained release of drugs, Nano. 02 (2007) 115–120. doi:10.1142/S1793292007000441.

[32] P. Yuan, P.D. Southon, Z. Liu, M.E. Green, J.M. Hook, S.J. Antill, C.J. Kepert, Functionalization of halloysite clay nanotubes by grafting with γ-aminopropyltriethoxysilane, J. Phys. Chem. C. 112 (2008) 15742–15751.

[33] R. Kamble, M. Ghag, S. Gaikawad, B.K. Panda, Halloysite Nanotubes and Applications: A Review., J. Adv. Sci. Res. 3 (2012).

[34] G.J. Churchman, P. Pasbakhsh, S. Hillier, The rise and rise of halloysite, Clay Miner. 51 (2016) 303–308.

[35] B. Szczepanik, P. Słomkiewicz, M. Garnuszek, P. Rogala, D. BanaŚ, K.-K. Aldona, I. Stabrawa, Effect of temperature on halloysite acid treatment for efficient chloroaniline removal from aqueous solutions, Clays Clay Miner. 65 (2017) 155–167.

[36] R.L. Frost, J. Kristof, Intercalation of halloysite: A raman spectroscopic study, Clays Clay Miner. 45 (1997) 551–563.

[37] B. Singh, R.J. Gilkes, An electron optical investigation of the alteration of kaolinite to halloysite, Clays Clay Miner. 40 (1992) 212–229.

[38] G.W. Brindley, M. Nakahira, Kinetics of Dehydroxylation of Kaolinite and Halloysite, J. Am. Ceram. Soc. 40 (1957) 346–350. doi:10.1111/j.1151-2916.1957.tb12549.x.

[39] G.W. Brindley, M. Nakahira, The Kaolinite-Mullite Reaction Series: II, Metakaolin, J. Am. Ceram. Soc. 42 (1959) 314–318. doi:10.1111/j.1151-2916.1959.tb14315.x.

[40] A.K. Chakraborty, Phase transformation of kaolinite clay, Springer, 2016.

[41] De Aza, X. Turrillas, M.A. Rodriguez, T. Duran, P. Pena, Time-resolved powder neutron diffraction study of the phase transformation sequence of kaolinite to mullite, J. Eur. Ceram. Soc. 34 (2014) 1409–1421. doi:10.1016/j.jeurceramsoc.2013.10.034.

[42] P. Ildefonse, R.J. Kirkpatrick, B. Montez, G. Calas, A.M. Flank, P. Lagarde, 27a1 mas nmr and aluminum x-ray absorption near edge structure study of imogolite and allophanes, Clays Clay Miner. 42 (1994) 276–287. doi:https://doi.org/10.1346/CCMN.1994.0420306.

[43]   Y.-F. Chen, M.-C. Wang, M.-H. Hon, Phase transformation and growth of mullite in kaolin ceramics, J. Eur. Ceram. Soc. 24 (2004) 2389–2397.

[44]   K. Okada, N. ŌTsuka, J. Ossaka, Characterization of Spinel Phase Formed in the Kaolin-Mullite Thermal Sequence, J. Am. Ceram. Soc. 69 (1986).

[45]   J. Sanz, A. Madani, J.M. Serratosa, J.S. Moya, S. Aza, Aluminum-27 and Silicon-29 Magic-Angle Spinning Nuclear Magnetic Resonance Study of the Kaolinite-Mullite Transformation, J. Am. Ceram. Soc. 71 (1988).

[46]   M. Bellotto, A. Gualtieri, G. Artioli, S.M. Clark, Kinetic study of the kaolinite-mullite reaction sequence. Part I: Kaolinite dehydroxylation, Phys. Chem. Miner. 22 (1995) 207–217. doi:10.1007/BF00202253.

[47]   A. Gualtieri, M. Bellotto, G. Artioli, S.M. Clark, Kinetic study of the kaolinite-mullite reaction sequence. Part II: Mullite formation, Phys. Chem. Miner. 22 (1995) 215–222. doi:10.1007/BF00202254.

[48]   H. Schneider, J. Schreuer, B. Hildmann, Structure and properties of mullite—A review, J. Eur. Ceram. Soc. 28 (2008) 329–344. doi:10.1016/j.jeurceramsoc.2007.03.017.

[49]   M.F. Serra, M.S. Conconi, G. Suarez, E.F. Agietti, N.M. Rendtorff, Firing transformations of an argentinean calcareous commercial clay, Cerâmica. 59 (2013) 254–261. doi:10.1590/S0366-69132013000200010.

[50]   M.S. Conconi, M.R. Gauna, M.F. Serra, G. Suarez, E.F. Aglietti, N.M. Rendtorff, Quantitative firing transformations of a triaxial ceramic by X-ray diffraction methods, Cerâmica. 60 (2014) 524–531. doi:10.1590/S0366-69132014000400010.

[51]   L. Andrini, M.R. Gauna, M.S. Conconi, G. Suarez, F.G. Requejo, E.F. Aglietti, N.M. Rendtorff, Extended and local structural description of a kaolinitic clay, its fired ceramics and intermediates: An XRD and XANES analysis, Appl. Clay Sci. 124–125 (2016) 39–45. doi:10.1016/j.clay.2016.01.049.

[52]   C.E. White, L.M. Perander, J.L. Provis, J.S.J. van Deventer, The use of XANES to clarify issues related to bonding environments in metakaolin: a discussion of the paper S. Sperinck et al., "Dehydroxylation of kaolinite to metakaolin-a molecular dynamics study," J. Mater. Chem., 2011, 21, 2118–2125, J. Mater. Chem. 21 (2011) 7007–7010. doi:10.1039/C1JM10379B.

[53]   C.E. White, J.L. Provis, D.P. Riley, T. Proffen, L.M. Perander, D. Van, Characterisation and description of the structure of metakaolin by total scattering, density functional theory, and X-ray spectroscopy, in: Concr. Repair Rehabil. Retrofit. III - Proc. 3rd Int. Conf. Concr. Repair Rehabil. Retrofit., Alexander, M. G., Beushausen, H. D., Dehn, F., Moyo, P. (Eds.), CRC Press, Cape Town, South Africa, 2012: pp. 1426–1432. https://books.google.com.ar/books?hl=es&lr=&id=nwbNBQAAQBAJ&oi=fnd&pg=PP1&dq=%22Characterisation+and+description+of+the+structure+of+metakaolin+by+total+scattering,+density+functional+theory,+and+X-ray+spectroscopy%22&ots=kFgycYUwQb&sig=Xq0vApIVbopT2YH12JmJkl7_IQQ#v=onepage&q=%22Characterisation%20and%20description%20of%20the%20structure%20of%20metakaolin%20by%20total%20scattering%2C%20density%20functional%20theory%2C%20and%20X-ray%20spectroscopy%22&f=false.

[54]   L. Andrini, R.M. Toja, M.R. Gauna, M.S. Conconi, F.G. Requejo, N.M. Rendtorff, Extended and local structural characterization of a natural and 800 C fired Na-montmorillonite–Patagonian bentonite by XRD and Al/Si XANES, Appl. Clay Sci. 137 (2017) 233–240.

[55]   D.C. Koningsberger, R. Prins, X-ray absorption: principles, applications, techniques of EXAFS, SEXAFS, and XANES, (1988).

[56]   G. Bunker, Introduction to XAFS: A Practical Guide to X-ray Absorption Fine Structure Spectroscopy, Cambridge University Press, 2010.

[57] B. Ravel, M. Newville, ATHENA, ARTEMIS, HEPHAESTUS: data analysis for X-ray absorption spectroscopy using IFEFFIT, J. Synchrotron Radiat. 12 (2005) 537–541.

[58] C. Duce, S.V. Ciprioti, L. Ghezzi, V. Ierardi, M.R. Tinè, Thermal behavior study of pristine and modified halloysite nanotubes, J. Therm. Anal. Calorim. 121 (2015) 1011–1019. doi:10.1007/s10973-015-4741-7.

[59] V. Viswabaskaran, F.D. Gnanam, M. Balasubramanian, Mullitisation behaviour of calcined clay–alumina mixtures, Ceram. Int. 29 (2003) 561–571. doi:10.1016/S0272-8842(02)00203-1.

[60] K.J.D. MacKenzie, R.H. Meinhold, I.W.M. Brown, G.V. White, The formation of mullite from kaolinite under various reaction atmospheres, J. Eur. Ceram. Soc. 16 (1996) 115–119. doi:10.1016/0955-2219(95)00143-3.

[61] L. Riber, H. Dypvik, R. Sørlie, R.E. Ferrell Jr, Clay minerals in deeply buried paleoregolith profiles, Norwegian North Sea, Clays Clay Miner. 64 (2016) 588–607.

[62] M.E. Ouahabi, L. Daoudi, F. Hatert, N. Fagel, Modified Mineral Phases During Clay Ceramic Firing, Clays Clay Miner. 63 (2015) 404–413.

[63] K. Okada, N. ŌTsuka, J. Ossaka, Characterization of Spinel Phase Formed in the Kaolin-Mullite Thermal Sequence, J. Am. Ceram. Soc. 69 (1986) C–251. doi:10.1111/j.1151-2916.1986.tb07353.x.

[64] J. Sanz, A. Madani, J.M. Serratosa, J.S. Moya, S. Aza, Aluminum-27 and Silicon-29 Magic-Angle Spinning Nuclear Magnetic Resonance Study of the Kaolinite-Mullite Transformation, J. Am. Ceram. Soc. 71 (1988) C418–C421. doi:10.1111/j.1151-2916.1988.tb07513.x.

[65] E. Joussein, Chapter 2 - Geology and Mineralogy of Nanosized Tubular Halloysite, in: P. Yuan, A. Thill, F. Bergaya (Eds.), Dev. Clay Sci., Elsevier, 2016: pp. 12–48. doi:10.1016/B978-0-08-100293-3.00002-9.

[66] D. Li, G.M. Bancroft, M.E. Fleet, X.H. Feng, Y. Pan, Al K-edge XANES spectra of aluminosilicate minerals, Mineralogical Society of America, 1995.

[67] T. Yamamoto, Assignment of pre-edge peaks in K-edge x-ray absorption spectra of 3d transition metal compounds: electric dipole or quadrupole?, X-Ray Spectrom. 37 (2008) 572–584.

[68] J.J. Rehr, A.L. Ankudinov, Progress in the theory and interpretation of XANES, Coord. Chem. Rev. 249 (2005) 131–140.

[69] E. Tamura, J. Van Ek, M. Fröba, J. Wong, X-Ray absorption near edge structure in metals: relativistic effects and core-hole screening, Phys. Rev. Lett. 74 (1995) 4899.

[70] C.E. White, J.L. Provis, T. Proffen, D.P. Riley, J.S.J. van Deventer, Density Functional Modeling of the Local Structure of Kaolinite Subjected to Thermal Dehydroxylation, J. Phys. Chem. A. 114 (2010) 4988–4996. doi:10.1021/jp911108d.

[71] C.E. White, K. Page, N.J. Henson, J.L. Provis, In situ synchrotron X-ray pair distribution function analysis of the early stages of gel formation in metakaolin-based geopolymers, Appl. Clay Sci. 73 (2013) 17–25. doi:10.1016/j.clay.2012.09.009.

[72] C.E. White, K. Page, N.J. Henson, J.L. Provis, In situ synchrotron X-ray pair distribution function analysis of the early stages of gel formation in metakaolin-based geopolymers, Appl. Clay Sci. 73 (2013) 17–25. doi:10.1016/j.clay.2012.09.009.

[73] L. Andrini, M.R. Gauna, M.S. Conconi, G. Suarez, F.G. Requejo, E.F. Aglietti, N.M. Rendtorff, Extended and local structural description of a kaolinitic clay, its fired ceramics and intermediates: An XRD and XANES analysis, Appl. Clay Sci. 124–125 (2016) 39–45. doi:10.1016/j.clay.2016.01.049.

[74] Y. Kato, K. Shimizu, N. Matsushita, T. Yoshida, H. Yoshida, A. Satsuma, T. Hattori, Quantification of aluminium coordinations in alumina and silica–alumina by Al K-edge XANES, Phys. Chem. Chem. Phys. 3 (2001) 1925–1929. doi:10.1039/B100610J.